BIOCHEMISTRY
including biophysical chemistry & molecular biology

Article

pubs.acs.org/biochemistry

Influence of Heme Post-Translational Modification and Distal Ligation on the Backbone Dynamics of a Monomeric Hemoglobin

Matthew P. Pond,[†] Ananya Majumdar,[‡] and Juliette T. J. Lecomte*[,†]

[†]T. C. Jenkins Department of Biophysics and [‡]Biomolecular NMR Center, Johns Hopkins University, Baltimore, Maryland 21218, United States

Supporting Information

ABSTRACT: The cyanobacterium *Synechococcus* sp. PCC 7002 uses a hemoglobin of the truncated lineage (GlbN) in the detoxification of reactive species generated in the assimilation of nitrate. In view of a sensing or enzymatic role, several states of GlbN are of interest with respect to its structure−activity relationship. Nuclear magnetic resonance spectroscopy was applied to compare the structure and backbone dynamics of six GlbN forms differing in their oxidation state [Fe(II) or Fe(III)], distal ligand to the iron (histidine, carbon monoxide, or cyanide), or heme post-translational modification (*b* heme or covalently attached heme). Structural properties were assessed with pseudocontact shift calculations. ^{15}N relaxation data were analyzed by reduced spectral density mapping (picosecond to nanosecond motions) and by inspection of elevated R_2 values (microsecond to millisecond motions). On the picosecond to nanosecond time scale, GlbN exhibited little flexibility and was unresponsive to the differences among the various forms. Regions of slightly higher mobility were the CE turn, the EF loop, and the H−H′ kink. In contrast, fluctuations on the microsecond to millisecond time scale depended on the form. Cyanide binding to the ferric state did not enhance motions, whereas reduction to the ferrous bis-histidine state resulted in elevated R_2 values for several amides. This response was attributed, at least in part, to a weakening of the distal histidine coordination. Carbon monoxide binding quenched some of these fluctuations. The results emphasized the role of the distal ligand in dictating backbone flexibility and illustrated the multiple ways in which motions are controlled by the hemoglobin fold.

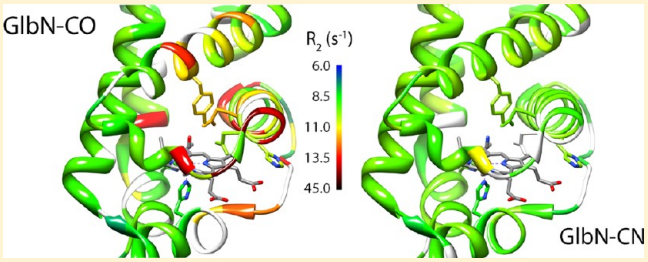

To date, more than 4500 protein sequences have been classified as hemoglobins.[1] Phylogenetic analyses of the superfamily identify three ancient lineages,[2,3] two of which contain proteins folding into the 3-over-3 (3/3) α-helical bundle illustrated by sperm whale myoglobin.[4] The third lineage is composed of proteins exhibiting a modified version of the canonical structure, termed a 2-over-2 version of the canonical structure (2/2) bundle.[5] These "truncated" hemoglobin domains are found in prokaryotes, unicellular eukaryotes, fungi, and plants.[3,6] Limited physiological evidence for several members of the lineage points to functional roles in processing reactive oxygen and nitrogen species,[3,7,8] activities that suggest versatility of structural and dynamic features within the superfamily. Here, we present a nuclear magnetic resonance (NMR) study of the hemoglobin from the cyanobacterium *Synechococcus* sp. PCC 7002 (GlbN, product of the *glbN* gene) focusing on the differential behavior of various forms of the protein and contributing to the elucidation of structure−function relationships in the 2/2 hemoglobin lineage.

GlbN differs from other hemoglobins not only in its shorter sequence and 2/2 topology but also in the bis-histidine coordination of the heme iron and the ability to undergo a post-translational modification (PTM) that attaches the heme covalently to the polypeptide.[9] These two traits are shared by the hemoglobin from the cyanobacterium *Synechocystis* sp. PCC 6803 (hereafter S6803GlbN), which has a sequence 59% identical with that of GlbN and has been extensively characterized in vitro.[10−16]

The post-translationally modified GlbN (denoted GlbN-A) contains a covalent bond between the Nε2 atom of His117 and the Cα atom of the heme 2-vinyl substituent.[12,17] This linkage is readily produced in preparations of the recombinant material by reduction of the heme iron.[12] GlbN isolated from *Synechococcus* cells is found mostly in the unmodified state (denoted GlbN-R) when the cells are grown under standard aerobic conditions, whereas the ratio of GlbN-A to GlbN-R is higher when the protein is extracted from cells grown under microoxic conditions.[8]

Figure 1A shows the structure of S6803GlbN-A with the proximal histidine (His70, at position F8 in the Perutz 3/3 nomenclature)[18] and distal histidine (His46, at position E10) coordinated to the iron. The binding of exogenous ligands displaces His46 and causes a large-amplitude structural reorganization (Figure 1B). In cyanomet and azidomet S6803GlbN-A, the tertiary rearrangement results in the

Received: May 13, 2012
Revised: June 22, 2012
Published: July 9, 2012

   dx.doi.org/10.1021/bi300624a | *Biochemistry* 2012, 51, 5733−5747

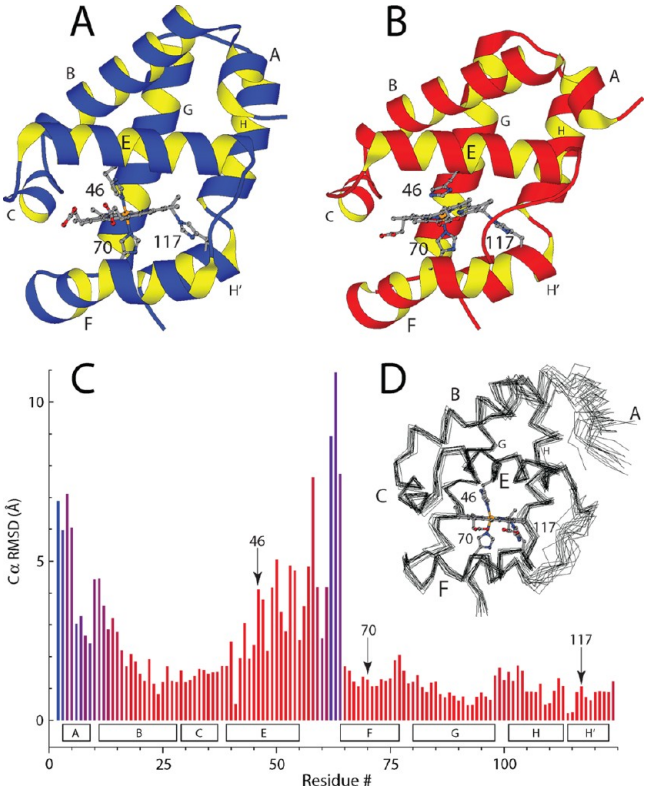

Figure 1. Crystal structures of S6803GlbN-A in (A) the ferric bis-histidine state (PDB entry 1RTX) and (B) the cyanomet state (PDB entry 1S69). Helices are labeled according to Perutz nomenclature.[18] (C) Pairwise Cα distances for the least-squares superimposition[20] of the two structures, as performed in the original comparison.[15] Vertical arrows indicate the location of His46, His70, and His117. (D) NMR structure of bis-histidine GlbN-A (PDB entry 2KSC). The bars in panel C are colored by Cα rmsd values (red for low and blue for high) in the 2KSC NMR structure.

formation of a distal hydrogen bond network involving TyrB10, GlnE7, and GlnE11 and the creation of solvent-to-heme tunnels wide enough to allow ligand access (Figure S1 of the Supporting Information).[15] The solution structure of GlbN-A presented in Figure 1C resembles the structure of S6803GlbN-A, and all evidence indicates that the same conformational transition takes place when ferric GlbN, with and without covalent heme attachment, binds cyanide.[19]

Access of ligands to the heme iron in globins has attracted attention since the early days of protein structure determination.[21] Decades of experimental studies of myoglobin have identified the major entry and exit pathway for diatomic ligands as passing by the distal histidine, which serves as a gate and traps small molecules in the heme cavity.[22−24] GlbN, with its transient tunnels coupled to distal ligation, offers a variation on the histidine gate mechanism and is expected to display internal motions relevant to activity in catalytic 2/2 hemoglobins.

In vivo data suggest direct participation of GlbN in protecting the bacterium from reactive oxygen/nitrogen species, possibly as a peroxynitrite detoxification enzyme.[8] As an enzyme or as a sensor, GlbN would need to visit different states. To gain an understanding of the relationship between motions and heme reactivity, it is therefore necessary to characterize multiple forms of the protein. We investigated GlbN backbone dynamics systematically as they were affected by heme ligation status, oxidation state, and heme PTM.

Throughout this study, each form is represented with the following string of properties: iron oxidation state, PTM state, distal ligand. In all cases, the proximal ligand is His70 and is omitted from the string. For instance, the ferric (oxidized or met), post-translationally modified, bis-histidine protein is termed Fe(III)GlbN-A-His. Table 1 lists the examined species and their spin states.

Table 1. GlbN Forms of Interest and Their Spin States

cross-linked (GlbN-A)	S	non-cross-linked (GlbN-R)	S
Fe(III)GlbN-A-His	$^1/_2$	Fe(III)GlbN-R-His	$^1/_2$
Fe(III)GlbN-A-CN	$^1/_2$	Fe(III)GlbN-R-CN	$^1/_2$
Fe(II)GlbN-A-His	0	—	
Fe(II)GlbN-A-CO	0	—	

We found that the PTM had an only modest impact on backbone fluctuations in ferric GlbN and that changes in the heme iron oxidation state altered motions on the microsecond to millisecond time scale. Within the same oxidation state, we also noted differences caused by the nature of the distal ligand. The observations highlight the notion that several factors influence the dynamics of GlbN and reinforce the fact that the properties of one form cannot be readily generalized to others, even if these are structurally closely related. These considerations are particularly important when examining ligand diffusion and allosteric effects in other hemoglobins and heme proteins.

MATERIALS AND METHODS

Protein Production and Purification. GlbN was obtained from overexpression of the *glbN* gene in BL21(DE3) cells grown in M9 medium.[9,25,26] Briefly, apoGlbN was purified from urea-solubilized inclusion bodies by being passed over a Sephadex G-50 Fine sizing column. The pure fractions were pooled, concentrated, and reconstituted with hemin chloride, resulting in Fe(III)GlbN-R-His. Further purification was achieved with a DEAE anion exchange column. GlbN-A was prepared by treating GlbN-R with a 5-fold excess of sodium dithionite for 5 min under microoxic conditions in the absence of exogenous ligand.[17] When necessary, oxidation to the ferric state was achieved via addition of an excess of potassium ferricyanide and passage over a Sephadex G-25 desalting column. All GlbN samples were lyophilized prior to being stored at −20 °C.

Preparation of GlbN Samples for NMR Analysis. Lyophilized GlbN samples were resuspended in 20 or 100 mM phosphate buffer (pH 7.2) containing 10% ^2H_2O. GlbN concentrations ranged from 1 to 2 mM as determined by UV−vis spectroscopy using extinction coefficients of 96 mM^{-1} cm^{-1} at 411 nm for Fe(III)GlbN-R-His and 87 mM^{-1} cm^{-1} at 409 nm for Fe(III)GlbN-A-His.[25] Fe(II)GlbN-A-His samples were prepared by reduction of Fe(III)GlbN-R-His or Fe(III)GlbN-A-His samples with an excess of dithionite. The glucose oxidase/D-glucose/catalase (GODCAT) oxygen-scavenging system[27] was used to maintain GlbN-A-His in the reduced state.[17] Fe(III)GlbN-CN samples were generated by adding a 50-fold molar excess of potassium cyanide to Fe(III)GlbN-R-His or Fe(III)GlbN-A-His. Fe(II)GlbN-A-CO samples were generated by gentle bubbling of CO in a Fe(III)GlbN-A-His solution followed by addition of a 5-fold molar excess of dithionite under microoxic conditions and further bubbling of CO. Fe(II)GlbN-A-CO was stable over the course of many

dx.doi.org/10.1021/bi300624a | *Biochemistry* 2012, 51, 5733−5747

days in a Shigemi NMR tube and did not require use of the GODCAT system.

NMR Spectroscopy. NMR spectra were recorded at 298 K on Bruker Avance, Bruker Avance II, or Varian Inova spectrometers, each equipped with a cryogenic probe and operating at a ^{1}H resonance frequency of 600.13, 600.53, or 799.70 MHz, respectively. ^{1}H chemical shifts were referenced to DSS through the water line at 4.76 ppm. Indirect referencing was applied with DSS Ξ values to obtain ^{15}N and ^{13}C shifts. Two- and three-dimensional NMR data sets were processed with NMRPipe[28] and analyzed with SPARKY.[29]

Standard pulse sequences[30] with a WATERGATE modification[31] were applied to measure ^{15}N R_1, ^{15}N R_2, and $\{^1H\}-^{15}N$ NOE. Because of the comparative nature of the study, complete ^{15}N relaxation analysis was performed at 14.1 T with additional ^{15}N R_2 data sets at 18.8 T as needed (see Discussion). Recycle delays were 3 s for R_1 experiments and 4 s for R_2 experiments, which were run with 0.9 ms delays between CPMG pulses. R_1 and R_2 values were determined from single-exponential fits to at least six data points. This was accomplished with the script Sparky2rate (J. P. Loria, Yale University, New Haven, CT) to provide data to the program Curvefit (A. G. Palmer, Columbia University, New York, NY). For error estimation, the jackknife procedure was preferred over the Monte Carlo method. ^{1}H saturation for the $\{^1H\}-^{15}N$ NOE measurements was achieved with a train of 180° WURST pulses,[32] spaced 10 ms apart, applied for either 4 or 7 s (control experiments demonstrated no significant difference between the two saturation periods). Reference spectra without ^{1}H saturation were conducted with 4 s delays between transients. Errors in $\{^1H\}-^{15}N$ NOE values were determined from the standard deviation of three consecutive measurements. 1D-TRACT data[33] were acquired to estimate the tumbling time of the protein in solution. Additional information concerning the collection and analysis of NMR data is presented in the Supporting Information.

Structural Calculations. In the absence of a three-dimensional structure for ligand-bound GlbN, a homology model was constructed using the structure of Fe(III)-S6803GlbN-A-CN (PDB entry 1S69).[34] The validity of this model was assessed by its ability to reproduce the pseudocontact shifts of the cyanide complexes. If the structure of carbonmonoxy GlbN ($S = 0$) is identical to the structure of cyanomet GlbN ($S = {}^1/_2$), then the difference in chemical shift

$$\Delta\delta_i = \delta_{obs,CN,i} - \delta_{obs,CO,i} \quad (1)$$

for proton i (several bonds remote from the iron to avoid contact contributions) is equal to $\delta_{pc,i}$, the pseudocontact shift at position i. The expression for $\delta_{pc,i}$ is[35,36]

$$\delta_{pc,i}(\text{calc}) = \frac{1}{12\pi r_i^3}\left[\Delta\chi_{ax}(3\cos^2\theta_i - 1) + \frac{3}{2}\Delta\chi_{rh}\sin^2\theta_i\cos 2\varphi_i\right] \quad (2)$$

where $\Delta\chi_{ax}$ and $\Delta\chi_{rh}$ are the axial and rhombic components of the susceptibility tensor, respectively, and r_i, θ_i, and φ_i are the atomic coordinates in the $\Delta\chi$ tensor frame. The $\Delta\chi$ tensor frame is related to the molecular frame by a Euler rotation matrix with angles α, β, and γ. The molecular frame was obtained by transforming the coordinates of the ligand-bound GlbN model to place the Fe atom at the origin, the x axis through the N atom of pyrrole C, the y axis through the N atom of pyrrole B, and the z axis through the Nε2 atom of the proximal histidine (His70). In excess of 200 ^{1}H $\Delta\delta_i$ values and the transformed coordinates were used as input to Numbat[37] to optimize the magnetic susceptibility tensor parameters (α, β, γ, $\Delta\chi_{ax}$, and $\Delta\chi_{rh}$) of the cyanide complexes with and without PTM. These $\Delta\delta_i$ values were for backbone amide H, Hα, and CβH$_3$ of alanine conserved in GlbN and S6803GlbN.

RESULTS

To investigate GlbN dynamics in the context of factors expected to control globin reactivity, three variables were altered: oxidation state, PTM status, and nature of the distal ligand. Reduction of the heme iron in the bis-histidine state causes the PTM to occur,[17] rendering the Fe(II)GlbN-R-His form inaccessible for study. Similarly, attempts to study Fe(II)GlbN-R-CO were hindered by conversion of the protein to Fe(II)GlbN-A-CO over the course of the NMR experiments. Furthermore, the reduced state of GlbN does not bind cyanide with appreciable affinity, and the oxidized state does not bind carbon monoxide. Thus, a total of six forms of GlbN could be studied (Table 1). A cursory examination of the NMR data suggested that the GlbN-His and GlbN-X conformations (where X is a non-histidine distal ligand) were endowed with distinct dynamic properties. The results were therefore grouped according to endogenous and exogenous ligation states, and the effects of iron oxidation state and PTM status are presented within these two contexts.

Resonance Assignments. To interpret the results of the ^{15}N relaxation data, ^{15}NH assignments were required. The data for Fe(III)GlbN-A-His, Fe(III)GlbN-R-His, and Fe(II)GlbN-A-His have been published previously (BMRB entries 16306, 16307, and 17947, respectively).[25,26,38] The assignments for Fe(II)GlbN-A-CO (BMRB entry 18422) were obtained by applying standard triple-resonance techniques to uniformly ^{13}C- and ^{15}N-labeled samples (see the Supporting Information). Homonuclear data and ^{15}N-separated NOESY and TOCSY data were adequate for the assignment of the backbone of Fe(III)GlbN-A-CN and Fe(III)GlbN-R-CN (BMRB entries 18423 and 18424, respectively) because of similarities with the assigned Fe(II)GlbN-A-CO spectra. In each GlbN-X case, all 121 backbone NH assignments were obtained with the exception of the Gly63 NH in the carbonmonoxy form. The annotated $^1H-^{15}N$ HSQC spectra of the six forms of GlbN are provided as Supporting Information (Figures S2–S7).

Structure of the Bis-Histidine Complexes. The structure of Fe(III)GlbN-A-His in solution has been determined (Figure 1D),[8] and NMR data support the notion that only small and localized perturbations occur upon formation of the heme–His117 cross-link.[8,25,26] Studies of Fe(II)GlbN-A-His show that reduction has no effect on the helical arrangement.[38] NMR data and crystal structures of S6803GlbN point to the same conclusions.[13−15] In view of these similarities, the NMR structure of Fe(III)GlbN-A-His was used as the model for all three bis-histidine complexes.

Structure of the GlbN-X Complexes. The conformational change caused by cyanide and azide binding has been documented in S6803GlbN-A.[14,15] It consists of a reorientation of the distal side of the heme bringing Tyr22 (B10) into contact with the ligand and swinging His46 toward the solvent (Figure 1A,B). ^{1}H/^{2}H isotope effects on the heme electronic structure in the cyanide complex of GlbN[19] along with NOE data and chemical shift analysis (vide infra) indicate that this conformational rearrangement is conserved in the two

dx.doi.org/10.1021/bi300624a | Biochemistry 2012, 51, 5733−5747

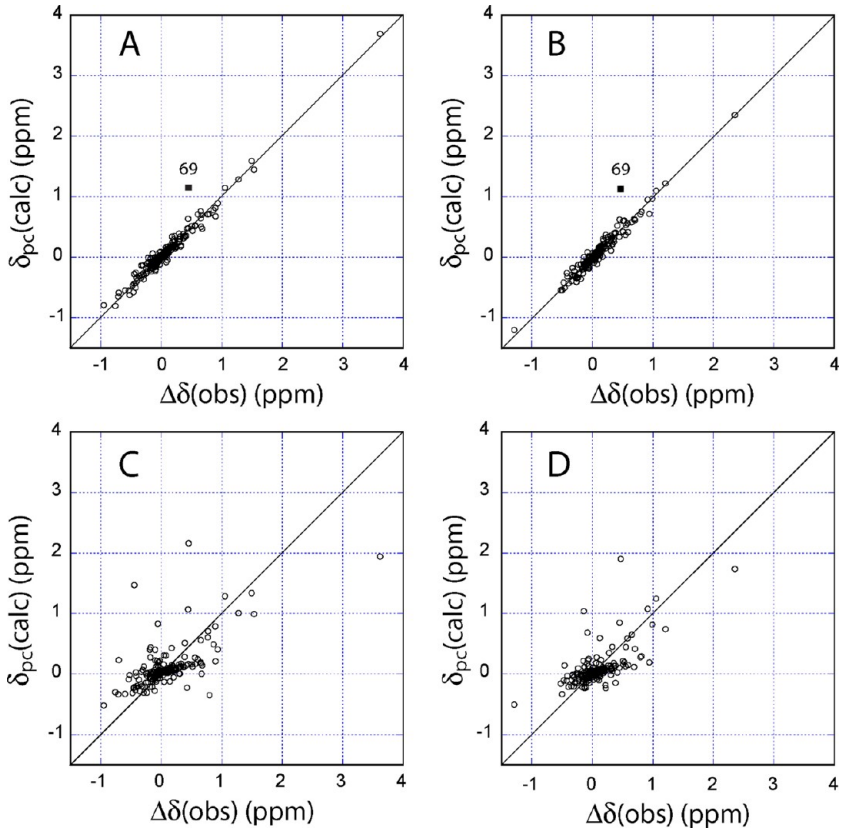

Figure 2. Comparison of observed and calculated pseudocontact shifts for (A) Fe(III)GlbN-R-CN and (B) Fe(III)GlbN-A-CN using Fe(II)GlbN-A-CO as the diamagnetic shift reference and the coordinates of a homology model based on the structure of Fe(III)S6803GlbN-A-CN. The solid diagonal line represents a perfect correlation. Linear regression returned the following: δ_{pc}(calc) = 0.97$\Delta\delta$(obs) − 0.01 with an R^2 of 0.97 (A), and δ_{pc}(calc) = 0.97$\Delta\delta$(obs) − 0.01 with an R^2 of 0.96 (B). The filled squares in panels A and B indicate the Ala69 CβH$_3$ group. The magnetic susceptibility tensor parameters are provided in the Supporting Information (Figure S9). (C and D) Same as panels A and B, respectively, when using the coordinates of Fe(III)GlbN-A-His instead of the homology model. δ_{pc}(calc) = 0.50$\Delta\delta$(obs) + 0.06 with an R^2 of 0.43 (C), and δ_{pc}(calc) = 0.57$\Delta\delta$(obs) + 0.03 with an R^2 of 0.47 (D).

cyanobacterial proteins. No structure is available for Fe(II)-S6803GlbN-A-CO; however, it is generally observed that carbonmonoxy and cyanomet complexes resemble each other. Here, our starting assumption was that all S6803GlbN-X and GlbN-X shared the same fold.

The secondary structure of Fe(II)GlbN-A-CO was inspected with TALOS+.[39] The calculated dihedral angles were found to match well those of Fe(III)S6803GlbN-A-CN (Figure S8 of the Supporting Information). The comparison of the GlbN-X complexes was refined using the pseudocontact shifts in the cyanomet forms (eq 2). The difference in the observed ^{1}H chemical shift [$\Delta\delta_i$ (see eq 1)] between Fe(III)GlbN-R-CN [or Fe(III)GlbN-A-CN] and Fe(II)GlbN-A-CO was obtained for backbone signals and conserved Ala CβH$_3$ groups. If the structures of the paramagnetic and diamagnetic forms are identical and this structure is used in the chemical shift computation, calculated and experimental values should match.

The correlation between observed $\Delta\delta_i$ values and shifts calculated with a model constructed from the X-ray structure of Fe(III)S6803GlbN-A-CN is presented in Figure 2A for Fe(III)GlbN-R-CN and Figure 2B for Fe(III)GlbN-A-CN. In both cases, the agreement was excellent. The main outlier was the CβH$_3$ group of Ala69 (F7), which was excluded from the fits. A few other nuclei in the proximity of the paramagnetic center also exhibited noticeable deviations. These sensitive reporters indicated that only small inaccuracies were present in the model and that the solution structure of GlbN-X was reliably represented by the fold of Fe(III)S6803GlbN-A-CN. Furthermore, when the bis-histidine structure (PDB entry 2KSC) was used instead of the GlbN-X homology model, the correlation coefficient dropped below 0.5 and the slope differed from unity (Figure 2C,D). These observations demonstrated the validity of the approach and confirmed that similar backbone structural changes occurred upon binding of cyanide or carbon monoxide. We therefore considered the homology model to be acceptable for the purpose of interpreting ^{15}N relaxation data collected on all three GlbN-X complexes.

The treatment described above focuses on backbone geometry as determined by pseudocontact shift calculations. Additional structural information came from the analysis of NOESY data. Dipolar contacts specific to the GlbN-X conformation were detected in all three such forms. The relevant NOEs were among Tyr5 (A helix), Gly57 (EF loop), and Gly10 (AB turn) (Figure S10 of the Supporting Information) and between Phe21 (B9) and Tyr22 (B10). The similarity of the two cyanomet forms and the carbonmonoxy form, however, did not extend to the immediate vicinity of the distal ligand. The side chain NH$_2$ groups of Gln43 (E7) and Gln47 (E11), which participate in the hydrogen bond network, were tentatively assigned in both cyanomet complexes, at chemical shifts close to those reported for H117A Fe(III)S6803GlbN-CN (Table S4 of the Supporting

dx.doi.org/10.1021/bi300624a | *Biochemistry* 2012, 51, 5733−5747

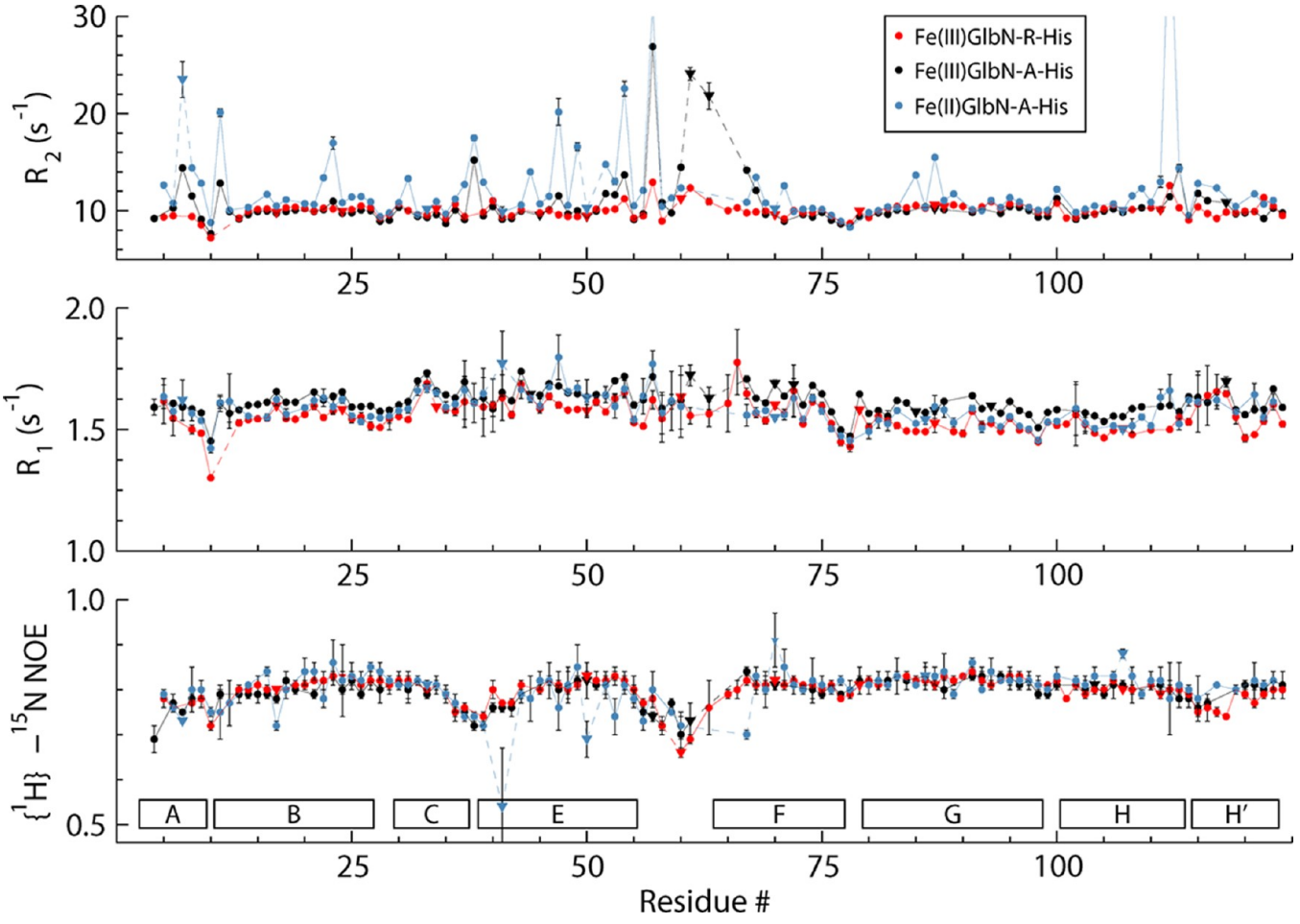

Figure 3. R_2 (top), R_1 (middle), and heteronuclear NOE (bottom) values for the three forms of GlbN-His at 14.1 T (pH 7.2, 298 K). Triangles indicate data points for which the uncertainty may be higher than what was calculated because of the spectral overlap or distortions. Dotted lines are used to connect triangles with other data and where consecutive points are missing. The R_2 values for Gly57 and Val112 in Fe(II)GlbN-A-His are off scale.

Information).[19] In Fe(II)GlbN-A-CO, only Gln43's NH_2 group, broad and with near-random coil chemical shifts, was identified (Figure S11 of the Supporting Information). Line broadening was also observed for several backbone amides in the E helix as an indication of a less well-defined structure.

Overall Rotational Correlation Times. Assessment of backbone dynamics by NMR spectroscopy requires knowledge of the overall tumbling time of the protein in solution. For this reason, rotational correlation times (τ_m) were estimated for the six GlbN forms using the 1D-TRACT experiment[33] under comparable experimental conditions (Figure S12 of the Supporting Information). Measured correlation times ranged from 7.3 ns for Fe(III)GlbN-R-His to 8.4 ns for Fe(II)GlbN-A-CO. The clustering of values was consistent with minimal influences from paramagnetic effects (vide infra). As previously observed,[40] the data revealed no oligomerization at millimolar concentrations of GlbN. Measurement of τ_m by this method was not expected to be accurate within the differences between forms [1.1 ns (see the Supporting Information)]. In addition, a τ_m value determined with the TRACT experiment is a lower-limit estimate based on a rigid body approximation. To account for this fact, the longest correlation times in each category [8.1 ns for Fe(II)GlbN-A-His and 8.4 ns for Fe(II)GlbN-A-CO] were selected to represent all GlbN-His and GlbN-X forms, respectively.

^{15}N Relaxation Measurements in GlbN-His. The ^{15}N relaxation data for GlbN-His are presented in Figure 3. R_1 and $\{^1H\}-^{15}N$ NOE values were nearly identical in all three forms, with the exception of the smaller R_1 values in Fe(III)GlbN-R-His. The lower rates were within the range of data acquired for different samples with different spectrometers and were not taken to indicate a change in overall tumbling or other dynamical processes. Further inspection of the $\{^1H\}-^{15}N$ NOE data indicated a small decrease in the CE turn and the EF loop, regions with few long-range contacts in the solution structure of Fe(III)GlbN-A-His. Several residues in the vicinity of the distal histidine also displayed lower $\{^1H\}-^{15}N$ NOE values in the ferrous form of the protein.

All three GlbN-His forms yielded high-quality R_2 data and pointed to more variability between forms than what is shown by the R_1 and $\{^1H\}-^{15}N$ NOE data. Fe(III)GlbN-R-His and Fe(III)GlbN-A-His displayed similar R_2 profiles, except that the former had lower values in the EF loop, in adjacent portions of helices E and F, and in helix A. The behavior of helix A in ferric GlbN was obscured by missing results for Ser3 and by overlap with other signals for Leu4 and Lys7 in Fe(III)GlbN-R-His. Inspection of the R_2 curves from the poorly resolved peaks did not permit comment on Leu4 but suggested that Lys7 had an R_2 similar to those of nearby residues. The trend for larger R_2 values detected in Fe(III)GlbN-A-His therefore appeared to be

dx.doi.org/10.1021/bi300624a | *Biochemistry* 2012, 51, 5733−5747

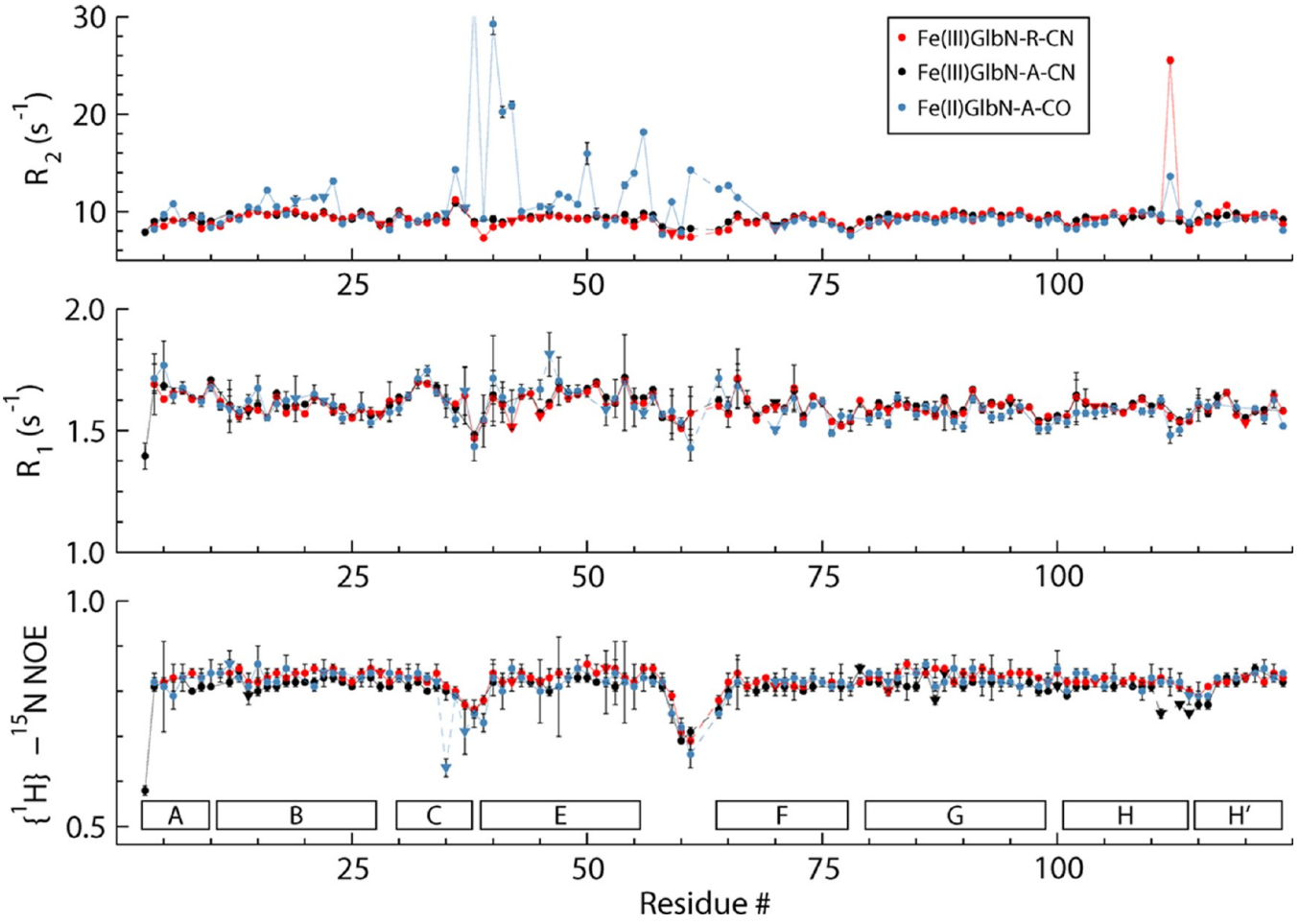

Figure 4. R_2 (top), R_1 (middle), and heteronuclear NOE (bottom) values for all three forms of GlbN-X studied at 14.1 T (pH 7.2, 298 K). As with GlbN-His, the differences are most pronounced in the R_2 measurements, and triangles mark data points for which the uncertainty may be higher than what was calculated. Dotted lines are used as in Figure 3. The R_2 value for Thr38 is off scale.

real. When compared to those of the ferric forms, R_2 values of Fe(II)GlbN-A-His were higher in several locations throughout the structure. A particularly large R_2 was noted for Val112 in Fe(II)GlbN-A-His (vide infra). In all three forms, the last 10 residues of the polypeptide chain had $\{^1H\}-^{15}N$ NOE, R_1, and R_2 values similar in magnitude to values measured in other parts of the protein, indicating that this region was stably fastened to the rest of the globin, likely through interactions involving Val121 and the heme.[8]

^{15}N Relaxation Measurements in GlbN-X. Figure 4 shows the results of the ^{15}N relaxation studies performed on the three available forms of GlbN-X. R_1 and $\{^1H\}-^{15}N$ NOE measurements were nearly independent of the nature of the ligand or the presence of the PTM. The similarity of $\{^1H\}-^{15}N$ NOE results between GlbN-His and GlbN-X included depression of values in the CE turn and the EF loop. Small differences were detected in helix A of GlbN-His and GlbN-X; these were likely due to specific interactions established with the beginning of the EF loop upon ligand binding. Unlike in the GlbN-His forms, assignment of Ser3 was possible in all three GlbN-X forms and provided additional evidence for altered behavior at the N-terminus. The only reliable relaxation data for Ser3, however, came from Fe(III)GlbN-A-CN, where decreases in both R_1 and $\{^1H\}-^{15}N$ NOE were noted.

The most striking observation from the GlbN-X ^{15}N relaxation data was the high R_2 values in helices B and E of Fe(II)GlbN-A-CO, which stood out against the relatively flat R_2 profiles of both cyanomet forms. Upon comparison of the R_2 rates in Fe(II)GlbN-A-His and Fe(II)GlbN-A-CO, R_2 enhancement was pronounced in the distal pocket of both forms of the protein but extended to additional residues in the Fe(II)GlbN-A-His complex. Upon comparison of ferric species, R_2 values for GlbN-CN were consistent with those of GlbN-His with the exception of helix A and parts of the EF loop. As observed in Fe(II)GlbN-A-His, the C-terminus appeared to be well fastened to the heme, and elevated rates were detected at position 112 in both Fe(III)GlbN-R-CN and Fe(II)GlbN-A-CO. The relatively low R_2 values measured for adjacent NH groups in five of the six forms of GlbN suggested that Val112 reported on the motion or ionization of a nearby side chain.

DISCUSSION

GlbN Structures. Prior work has shown that the three forms of GlbN-His have nearly indistinguishable secondary and tertiary structures.[8,25,26,38] The pseudocontact shift analysis of GlbN-X supported the idea that the crystal structure of Fe(III)S6803GlbN-A-CN provided a suitable model for the backbone conformation of all three forms of GlbN containing an exogenous ligand. Because no side chain chemical shifts (other than selected Ala CβH$_3$ groups) were included in the analysis and some key residues (e.g., Gln47) were not detected in all complexes, several important features were not captured

dx.doi.org/10.1021/bi300624a | *Biochemistry* 2012, 51, 5733−5747

by the homology model. For example, the details of the distal hydrogen bond network and of contacts involving the heme propionates remain undefined. Nevertheless, the magnetic susceptibility tensor orientation appeared to be well-defined by the backbone shifts. The tilt of the z axis with respect to the heme normal (β) was 5° for Fe(III)GlbN-R-CN and 9° for Fe(III)GlbN-A-CN, indicating a cyanide ligand with a C−N bond almost normal to the heme plane[36] as observed in Fe(III)S6803GlbN-A-CN.[15]

Variability in ligand−protein interactions has been observed for 2/2 globins despite nearly identical structural contexts. A comparison of *Chlamydomonas eugametos* hemoglobin (*Ce*Hb) and S6803GlbN illustrates the point. These two proteins contain TyrB10, GlnE7, and GlnE11. Resonance Raman data show that in the oxy state *Ce*Hb and S6803GlbN have strong hydrogen bonds with dioxygen and share unusual vibrational signatures, whereas in the carbonmonoxy state, the two proteins have little to no side chain interaction with bound carbon monoxide.[10,41−43] The cyanomet structures overlap with an rmsd of 0.75 Å (optimized by UCSF Chimera,[20] value over 110 Cα pairs), and the match is close for residues contacting the heme; however, they differ in the tilt of the cyanide C−N axis relative to the heme normal (Figure S13 of the Supporting Information) and therefore the details of the distal hydrogen bond network, as well.[15,44]

Although the level of identity with S6803GlbN is higher for GlbN (59%) than *Ce*Hb (45%), differences in behavior are still apparent. Binding of carbon monoxide to the reduced state of both cyanobacterial proteins retards the formation of the heme−His117 cross-link, presumably because of FeCO back-bonding and diminished electron density on the reactive vinyl.[17] However, preliminary observations at neutral pH (not shown) indicated that Fe(II)S6803GlbN-R-CO was stable for days, whereas Fe(II)GlbN-R-CO converted to Fe(II)GlbN-A-CO over the course of several hours. The observation suggests that distinct ligand−side chain interactions may exert subtle influences on reactivity. These influences may not be directly apparent in the structures.

Paramagnetic Contribution to Relaxation. The influence of a paramagnetic center on the chemical shift and relaxation rates of nearby nuclei has been extensively studied.[45−47] It is generally observed that, for an $S = {}^1/_2$ heme, the unpaired electron has a negligible influence on the R_1 and $\{^1H\}-^{15}N$ NOE values of nuclei outside of a 7 Å radius around the iron.[48,49] The only backbone amides inside of this radius are those of Phe50 and His70 in the GlbN-His structure and His70 in the GlbN-X structure. Figures 3 and 4 show that those residues did not deviate from the trend established by adjacent backbone positions. Thus, contributions from paramagnetism were ignored in R_1 and $\{^1H\}-^{15}N$ NOE data sets.

Distinguishing between conformational exchange (R_{ex}) and paramagnetic contributions to R_2 is more challenging. The contribution from Curie spin relaxation increases with the square of the magnetic field strength, as does R_{ex} in the fast exchange regime, and pseudocontact contributions can alter the magnitude of changes in chemical shift occurring during exchange events.[50] The diamagnetic forms of GlbN exhibited *higher* R_2 values than the paramagnetic forms, which suggested that the observed increases were due to increases in R_{ex} in the former species. Additionally, the flat R_2 profiles in helix F of all four paramagnetic forms of GlbN argued against a significant influence from the unpaired electron. For further confirmation, R_2 data sets were collected at 18.8 T to inspect field dependence. Fe(III)GlbN-A-CN was an ideal test case because of the apparent lack of R_{ex} contributions to the R_2 values. The 18.8 T data set demonstrated no significant increases in R_2 beyond the expected static field response (Figure S14 of the Supporting Information). A similar comparison was conducted for Fe(III)GlbN-A-His (Figure S15 of the Supporting Information) and is discussed in more detail in the Supporting Information. From these data, it appeared that contributions to R_2 from paramagnetism were negligible over the whole backbone.

Approach to Relaxation Data Analysis. The analysis of ^{15}N relaxation data took advantage of the high degree of structural similarity within each of the two GlbN contexts (GlbN-His or GlbN-X), allowing for an evaluation of the general features of GlbN backbone dynamics. The results are best interpreted in terms of relative changes in fast motions (picosecond to nanosecond time scale) and slow motions (microsecond to millisecond time scale) as a function of the position along the sequence. We opted to use different approaches to assess the motions on these two time scales.

To gauge the fast motions, we chose the reduced spectral density mapping approach[51,52] and used the equations

$$J(0.87\omega_H) = \frac{R_x}{5a} \tag{3}$$

$$J(\omega_N) = \frac{R_1}{b} - \frac{7R_x}{5b} \tag{4}$$

where $a^{1/2} = (\mu_0 h \gamma_H \gamma_N)/(16\pi^2 r_{NH}{}^3)$, $b = 3a + (\omega_N \Delta\sigma)^2/3$, $R_x = (\gamma_N/\gamma_H)(\mathrm{NOE} - 1)R_1$, μ_0 is the permeability of free space, h is Planck's constant, r_{NH} is the N−H bond length, $\Delta\sigma$ is the chemical shift anisotropy of the ^{15}N nucleus, and γ_H and γ_N are the gyromagnetic ratios of ^1H and ^{15}N, respectively. An ω_N of 60.8 MHz, a $\Delta\sigma$ of −160 ppm, and an r_{NH} of 1.02 Å were used. Alternate choices of $\Delta\sigma$ or r_{NH} values had no appreciable effect on the interpretation of the data (not shown). Although the procedure limits the analysis with respect to squared order parameters and internal correlation times, such as obtained with ModelFree,[53] it eliminates fitting errors and incorrect assumptions concerning the form of the spectral density function[54] and provides a suitable framework for inspecting relative changes among different forms of GlbN. In addition, because the mapping relies only on R_1 and $\{^1H\}-^{15}N$ NOE measurements, it is not subject to contributions from R_{ex} terms, and microsecond to millisecond time scale motions do not enter the analysis.

To identify residues exhibiting slow (microsecond to millisecond) motions, we favored a straightforward search for R_2 values exceeding two standard deviations from a trimmed average R_2 value. For GlbN-His, 16 points were removed from each side of the distribution, yielding a 5% trimmed average of 10.4 ± 1.1 s^{-1} and a selection criterion of R_2 of >12.6 s^{-1}; for GlbN-X, 10 points were removed from each side of the distribution, yielding a 3% trimmed average of 9.4 ± 0.8 s^{-1} and a selection criterion of R_2 of >11.0 s^{-1}. The consistency of R_2 rates over the majority of the backbone NH groups in all six forms and the response observed in R_2 data sets collected at 18.8 T (see the Supporting Information) reinforced the validity of the analysis. We also examined R_2/R_1 ratios. In ideal cases, internal motions on the picosecond to nanosecond time scale affect R_1 and R_2 similarly, and deviations from the trimmed R_2/R_1 average are due to R_{ex}. In practice, several factors conspire to affect the local ratios, including diffusional properties and a

dx.doi.org/10.1021/bi300624a | *Biochemistry* 2012, 51, 5733−5747

disparity in the influence of fast internal motions.[55,56] Here, contributions from anisotropic diffusion were expected to be similar within the GlbN-His group and within the GlbN-X group. Uncertainty in the selection procedure arises if a residue is systematically selected in all three proteins belonging to the same group. Only Val36 in GlbN-X met this criterion. In addition, observed R_1 and $\{^1H\}-^{15}N$ NOE values indicated that picosecond to nanosecond internal motions were limited (see below) and that relative errors in the cancellation of these contributions could be ignored. The deviating R_2/R_1 values identified by this method, including that for Val36, were large enough to make the influence of sources other than R_{ex} unlikely. Structure-based hydrodynamic calculations[57] were consistent with this interpretation and are detailed in the Supporting Information (Figures S17–S20).

The conservative R_2 selection approach focused on regions of GlbN where unambiguous changes in behavior took place. Interpretation of subtle changes with the Lipari–Szabo formalism[58] was not attempted because of the sensitivity to the selection of constants, motional models, and diffusion tensor. The R_2 and R_2/R_1 selection methods agreed on a total of 51 instances of microsecond to millisecond motions (Table S3 of the Supporting Information). Ten additional instances were identified by one method or the other. Each of these was retained as significant as each was located in regions of the protein where nearby residues exhibited a reliable enhancement of microsecond to millisecond motions [e.g., in Fe(II)GlbN-A-His, residues Asn37 and Thr38 were selected by the R_2 method and only Thr38 was selected by the R_2/R_1 method].

The procedures applied here were consolidated by the comparison of multiple protein forms. Thus, only a few data sets were required at a second static field to secure the interpretation of the results. Relaxation dispersion experiments outside the scope of this study will define the time scale of the motions and perhaps reveal that additional residues should be included in the slow-motion category.

Picosecond to Nanosecond Motions in GlbN. The results of the reduced spectral density analysis can be visualized with plots of $J(0.87\omega_H)$ [henceforth $J(\omega_H)$] versus $J(\omega_N)$.[59] Two representative such plots are shown in Figure 5. The black contour lines are the theoretical J traces for rigid isotropic tumbling with correlation times (t) ranging from 1 ps to 1 μs, given by

$$J(\omega_i)^{(\mathrm{rigid})}(t) = \frac{2}{5}\frac{t}{1+\omega_i^2 t^2} \quad (5)$$

To facilitate interpretation of the data, green lines are drawn that depict the variation of the calculated $J(\omega)$ values according to the Lipari–Szabo model-free formalism

$$J(\omega) = \frac{2}{5}\left[\frac{S^2\tau_m}{1+\omega_i^2\tau_m^2} + \frac{(1-S^2)\tau}{1+\omega_i^2\tau^2}\right] \quad (6)$$

where S^2 is the order parameter varying from 1 to 0 at the τ_m of GlbN-His or GlbN-X, and τ was arbitrarily set to 200 ps (in eq 6, $\tau^{-1} = \tau_m^{-1} + \tau_e^{-1}$ and τ_e is the correlation time of internal motion). These plots represent a simplified picture of picosecond to nanosecond dynamics and are insensitive to the possible effects from anisotropic diffusion or internal motions on time scales approaching τ_m.

All $[J(\omega_N),J(\omega_H)]$ points clustered within the same region of the plots, near the coordinates corresponding to the rigid body, and in good agreement with the rotational correlation times

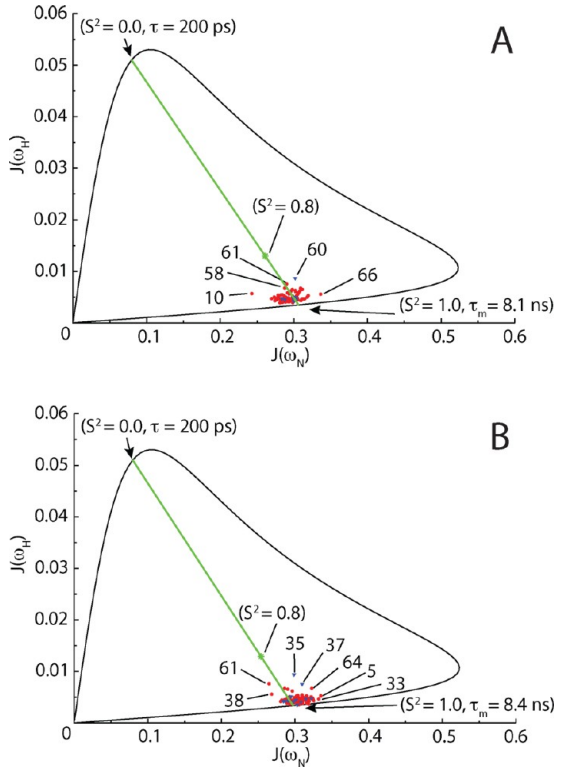

Figure 5. $J(\omega)$ plot for (A) Fe(III)GlbN-R-His and (B) Fe(II)GlbN-A-CO. The clustering of values near the τ_m suggests little internal motion on the picosecond to nanosecond time scale. Points represented by triangles in Figures 3 and 4 are colored blue.

estimated by the TRACT experiments. The same behavior was observed in the four other GlbN complexes (Figure S21 of the Supporting Information). A few minor outliers were noted, which tended to occur in the CE and EF regions. Overall, the data showed highly restricted N–H vectors (high S^2) on the picosecond to nanosecond time scale in all six forms of GlbN. Backbone rigidity on this time scale has also been observed in the 2/2 hemoglobin from *Mycobacterium tuberculosis* (trHbN) with cyanide bound,[60] the hemoglobin from *Glycera dibranchiata* in the carbonmonoxy form,[61] and adult human hemoglobin in both the deoxy and carbonmonoxy forms.[62] This uniform trend draws attention to slower, distinctive motions.

Microsecond to Millisecond Motions in GlbN-His. Figure 6 illustrates the distribution of R_2 values in the three GlbN-His forms. The data were consistent with similar microsecond to millisecond motions in Fe(III)GlbN-R-His and Fe(III)GlbN-A-His except in the EF and A regions, where cross-linking appeared to enhance mobility. Alteration of EF loop dynamics as a result of the PTM may be due to stress applied to the axial ligands and consequent distortion of the heme cavity. We have reported that lowering the pH below neutral sharpens the signals of this loop.[26] Inspection of this region of the protein identifies the heme propionates as candidates for acid–base equilibria. Neutralization of these functionalities may cause local reorganization.

A similar repositioning and transmission mechanism can be considered for helix A. The crystal structure of Fe(III)-S6803GlbN-A-His shows a helix A fastened to helix E by hydrophobic interactions involving Leu4, Leu8, Leu51, and Phe55. The adjacent Phe50 and Tyr53 contact the heme near

dx.doi.org/10.1021/bi300624a | *Biochemistry* 2012, 51, 5733–5747

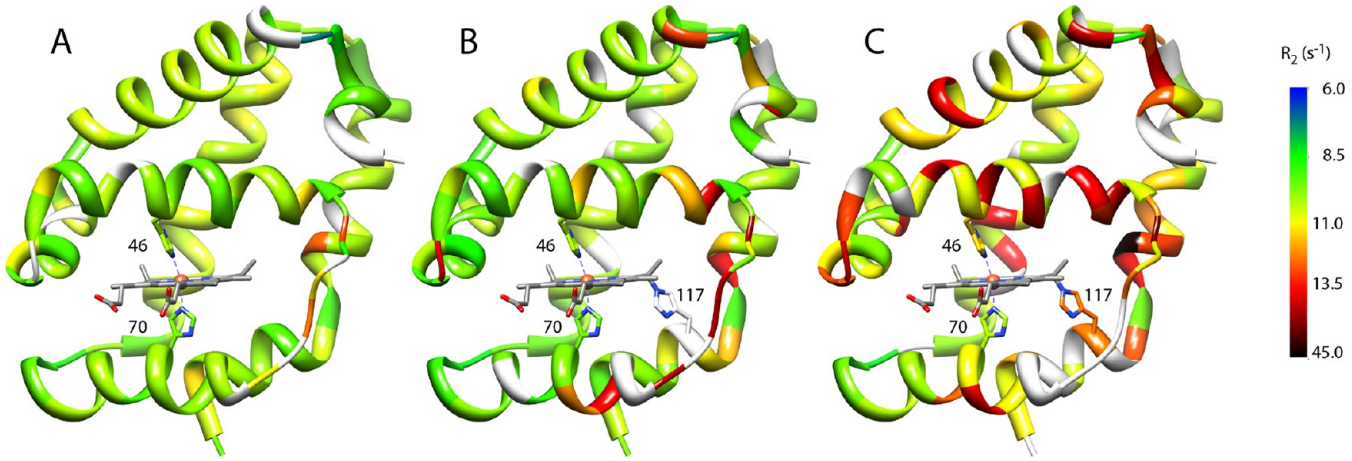

Figure 6. R_2 values measured in (A) Fe(III)GlbN-R-His, (B) Fe(III)GlbN-A-His, and (C) Fe(II)GlbN-A-His and plotted on the structure of Fe(III)GlbN-A-His (PDB entry 2KSC). Increased microsecond to millisecond motions (orange-red) are noted near the EF loop and in helix A of Fe(II)GlbN-A-His. In Fe(II)GlbN-A-His, the enhancement is distributed throughout the structure with a preference for the distal side. Key histidines are colored by backbone R_2.

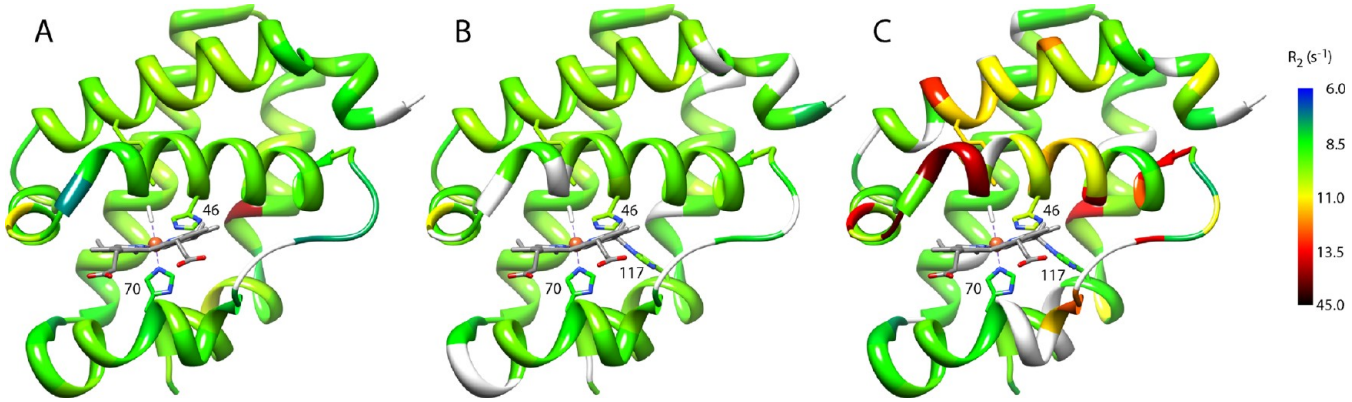

Figure 7. R_2 values measured for (A) Fe(III)GlbN-R-CN, (B) Fe(III)GlbN-A-CN, and (C) Fe(II)GlbN-A-CO and plotted on the structural model of GlbN-X. The higher R_2 values in helices B and E of Fe(II)GlbN-A-CO relative to the cyanomet forms indicated a localized increase in microsecond to millisecond backbone motions. Key histidines are shown as in Figure 6.

the site of the PTM, and it is in this region of helix E of GlbN that motions on the microsecond to millisecond time scale were registered. We note that the solution structure of Fe(III)GlbN-A-His (Figure 1) has a blurred N-terminus because of sparse NMR information, as was noticed in the solution ensemble of Fe(III)S6803GlbN-R-His.[13] Thus, helix A and the A−E interface, along with the EF loop, stand out as structural features particularly prone to fluctuating in response to chemical modification and changes in solution conditions.

When compared to the two ferric forms, Fe(II)GlbN-A-His experienced a significant increase in microsecond to millisecond motions. In fact, Fe(II)GlbN-A-His exhibited more regions of enhanced microsecond to millisecond motion than any of the other five forms studied. Figure 6 reveals a bias for flexibility on the distal side of the heme and in other areas surrounding the heme. It is noteworthy that the distal histidine is expected to have a lowered affinity for the iron in the reduced state,[63] a point to which we will return. It should also be specified that we have found no evidence of a significant population of a five-coordinate ferrous form in NMR[38] and optical spectra.[9]

Microsecond to Millisecond Motions in GlbN-X. Figure 7 maps the GlbN-X R_2 values onto the structural homology model. Whereas heme PTM had little effect on the cyanomet complex, the switch from Fe(III)-CN to Fe(II)-CO had noticeable consequences. In the latter form, an enhancement of slow motions was observed for helix B, helix E, and the EF loop. The increases in the EF loop extended to the adjacent residues in helices E and F, as observed in Fe(III)GlbN-A-His, but were not detected in helix A. The altered behavior may be related to the formation of strong interactions between helix A and the N-terminal end of the EF loop in GlbN-X (Figure S10 of the Supporting Information). Compared to that of Fe(II)GlbN-A-His, the enhancement was not as widespread, leading to the conclusion that in the Fe(III) and Fe(II) states, the presence of an exogenous ligand attenuated this type of motion.

It is likely that specific side chain contacts with the exogenous ligand are responsible for the distinct properties of the cyanomet and carbonmonoxy complexes. In the cyanomet complex, the distal hydrogen bond network is stably formed, but in the carbonmonoxy complex, line broadening was evidence of local fluctuations. This observation was consistent with the absence of interactions between protein and bound carbon monoxide inferred from resonance Raman data in S6803GlbN.[10] The GlbN NMR results, however, did not permit us to distinguish between the complete absence of interactions with bound carbon monoxide and the transient formation of contacts, as described for *M. tuberculosis* trHbN.[43]

dx.doi.org/10.1021/bi300624a | *Biochemistry* 2012, 51, 5733−5747

The comparison of GlbN relaxation data presented above is useful in assessing the significance of the results and in illustrating the complicated motional landscape of GlbN. In what follows, the data are inspected in the context of other heme proteins and with attention to specific chemical features.

Effect of the Heme−Protein Cross-Link. Few heme proteins have been compared with and without heme covalent attachment,[64−69] and among these, fewer yet have been studied for their dynamic properties. Of note is the artificial R98C variant of cytochrome b_{562}, which contains a single heme−protein covalent linkage. The consequence is an increase in the number of backbone NHs exhibiting fluctuations, presumably because of the strain imposed by the linkage.[70] In contrast, the effect of the cross-link in GlbN dynamics was minimal in the ferric GlbN-His and ferric GlbN-X states. $^{1}H-^{15}N$ HSQC data collected on H117A Fe(II)GlbN-His [as a substitute for wild-type Fe(II)GlbN-R-His] and compared to those of wild-type Fe(II)GlbN-A-His support the idea that the the cross-link also has a minor effect in the reduced state.[38]

The effect of the cross-link has been investigated previously by amide $^{1}H/^{2}H$ exchange (HX) experiments,[25] which provide a complementary view of backbone fluctuations. In Fe(III)-GlbN-A-His, HX is measurably retarded with respect to free peptide rates in the C-terminal half of helix B, helix C, the C-terminal half of helix E, scattered locations in helix F, most of helix G, and helix H outside of the kink centered at position 115. These regions correspond approximately to those where the $\{^{1}H\}-^{15}N$ NOEs are highest (Figure S22 of the Supporting Information). Conversely, hydrogens exchanging completely within the first 13 min of exposure to $^{2}H_2O$ at neutral pH were found in regions with depressed $\{^{1}H\}-^{15}N$ NOEs. The same applied to Fe(III)GlbN-R-His, except for the end of helix H (low levels of protection and high NOEs). A less well-defined correspondence between HX rates and R_2 was observed (see below), whereas no relation was expected with R_1 as this parameter was nearly uniform throughout the sequence.

A detailed comparison of HX data shows a trend for anisotropic redistribution of HX rates upon PTM, with a bias for an increased level of protection on the proximal side and a decreased level of protection on the distal side in GlbN-A.[25] Variations in R_2 did suggest a modest readjustment of dynamic properties caused by heme attachment, but there was no obvious connection to the changes in HX behavior. The absence of direct correlation is not surprising when one considers that distinctly different dynamic situations give rise to relaxation and exchange.[71] The redistribution of HX rates on cross-linking is likely to reflect changes in the frequency of rare excursions to exchange competent states. These changes would be undetectable with the relaxation method.

Discrepancies between relaxation and HX data can also be observed when helical elements undergo rigid body motions preserving hydrogen bond strength,[61] an example of which may be offered by helix C. Overall, the HX and relaxation data agreed that residues 70−111 (second half of helix F to the kink in helix H) were the most dynamically stable. The variable response at the C-terminus therefore suggested that the PTM quenched rare excursion events in this region of ferric GlbN-His.

Bis-Histidine Ligation and Redox State Effects. A recurring question about bis-histidine heme proteins concerns the factors that control the lability of the heme axial ligands, i.e., what distinguishes a gas sensor or an enzyme from an electron transport protein. The free energy of the state containing a displaced histidine relative to the free energy of the bis-histidine form[72] and the strength of the distal His−Fe bond[73] are two relevant characteristics. Systematic studies of histidine ligation in synthetic heme peptides have shown that the axial histidine second to coordinate a ferric iron has a higher affinity than the first, whereas in the ferrous state, the affinity order is reversed and leads to holoprotein destabilization.[63] This appears to be the hallmark of bis-histidine sensors. In contrast, the electron transport protein cytochrome b_5 is more stable in the ferric than the ferrous state, in a reversal attributed to significant influences from the protein matrix. We have observed that H117A Fe(II)GlbN loses the heme group more readily than H117A Fe(III)GlbN,[38] which aligns GlbN with sensors and enzymes.

Reduction of GlbN resulted in elevated R_2 values (Figure 6), whereas cytochrome b_5 becomes more rigid on the microsecond to millisecond time scale in the ferrous state.[48] The opposite responses of GlbN and cytochrome b_5 point to the impact of axial coordination strength on microsecond to millisecond motions. Redistribution of charges involving the heme propionates and reorganization of the solvation layer have also been invoked to explain the dependence of backbone flexibility on oxidation state in cytochrome b_5.[74] These effects may combine with axial histidine coordination strength to modulate dynamics in GlbN. It is interesting that, although the majority of bis-histidine globins are able to bind dioxygen and carbon monoxide to ferrous heme, exceptions have come to light.[75] This recent discovery demonstrates the ability of the globin fold not only to provide a sixth ligand to the iron but also to render it nondisplaceable as in cytochrome b_5. Dynamic studies of these globins will offer a new facet to the issue of axial histidine lability.

Carbonmonoxy versus Cyanomet GlbN. Cyanide and carbon monoxide are isosteric and isoelectronic. As a result, they are often used to compare the properties of ligand-bound hemoproteins in different oxidation states. Because of the stability of the complexes they form, they are also studied as surrogates for O_2-bound states, although there are obvious limitations to this approach.[76−78] In GlbN-X, the similarities between the cyanomet and carbonmonoxy complexes included tertiary structure and picosecond to nanosecond time scale motions but broke down when microsecond to millisecond time scale motions were considered, presumably because of weak interactions between the protein and carbon monoxide. Distinct cyanomet and carbonmonoxy GlbN properties were also evidenced by ^{19}F NMR spectroscopy in protein containing 3-fluorotyrosine at position B10,[79] the cyanomet state yielding sharp lines and the carbonmonoxy state yielding a broad and heterogeneous spectrum. These side chain observations reinforce a connection between the microsecond to millisecond time scale dynamics of GlbN and the nature of the distal ligand.

Functional Implications. *Post-Translational Modification.* The data indicated that a purely structural or dynamic role for the unusual His−heme bond was unlikely. As mentioned above, the proportion of GlbN with covalently attached heme is higher when *Synechococcus* sp. PCC 7002 cells are grown under microoxic conditions.[8] Because microoxic conditions also favor the production of heme oxygenases,[80] cross-link formation may be a necessary feature to eschew heme-degrading enzymes. This interpretation extends the view that the role of heme attachment is to prevent heme dissociation in the ferrous state.[16] Other properties, including iron redox potential[38] and stability of certain heme ligation states [e.g., Fe(II)GlbN-NO],

dx.doi.org/10.1021/bi300624a | *Biochemistry* 2012, 51, 5733−5747

are also adjusted by the cross-link and may modulate activity as demanded by cellular conditions.

Distal Ligand. Wild-type GlbN in the bis-histidine state is less susceptible to oxidative damage caused by H_2O_2 than variants that have His46 replaced with a noncoordinating residue.[17] The ability to block the distal site offers an advantage in vivo given the conditions under which GlbN functions.[8] His46 coordination also influences the regiospecificity of the PTM[17] and facilitates electron transfer.[38] The latter property may be relevant to a catalytic cycle in which ferrous iron delivers an electron to a substrate and needs to be re-reduced.

The physiological ligands of GlbN have not been identified. Current hypotheses focus on HOONO, NO, and O_2.[8] CO present in the cell may also associate with GlbN in some functional capacity. NO and O_2 studies are in progress to test the impact of the hydrogen bond with TyrB10[10,81] and discern dynamic differences between the two complexes. Figure 8 illustrates the heme pocket of Fe(III)S6803GlbN-A-CN with the residues participating in the hydrogen bond network colored by R_2 value as in Figure 7. It is interesting that regions with increased dynamics in Fe(II)GlbN-A-CO were found near the main ligand access tunnel identified with the cyanomet S6803GlbN structure.[15] The backbone motions appeared to reflect the loosening of the distal hydrogen bond network in Fe(II)GlbN-A-CO. In this complex, structural fluctuations controlled by the nature of one ligand may be linked to the ease of diffusion of another, as molecular dynamic simulations indicate for trHbN from *M. tuberculosis*.[60,82−85]

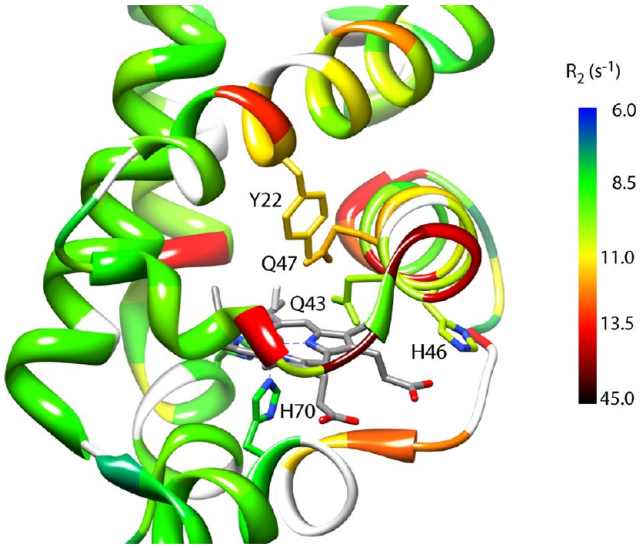

Figure 8. R_2 values of Fe(II)GlbN-A-CO plotted on the crystal structure of Fe(III)S6803GlbN-A-CN (PDB entry 1S69). The locations of the side chains involved in the hydrogen bond network and the key histidines are marked and colored by backbone R_2 value. The increased microsecond to millisecond motions (appearing yellow-red) are predominately found near the residues involved in the distal hydrogen bond network.

The importance of dynamics in hemoglobin was originally proposed for the access of O_2 to the iron.[21] Recently, the possibility was raised that entropic effects manifested in fluctuations associated with different ligation states play a determining role in the allosteric mechanism of adult human hemoglobin.[62,86] Our GlbN results reiterate that backbone dynamics can be sensitive to the identity of the distal ligand and that motional perturbations can occur at a distance from the iron.

Conformational States. Structures of GlbN-like proteins (group I 2/2 hemoglobins) are available from various organisms: *M. tuberculosis*,[87] *C. eugametos*,[44] *Paramecium caudatum*,[44] and *Tetrahymena pyriformis*.[88] These structures all contain an exogenous ligand and have the topological features of cyanomet S6803GlbN. Models of the ligand-free ferrous *M. tuberculosis* trHbN[89] do not suggest that a sixth ligand to the iron is necessary for the protein to adopt the ligand-bound conformation. As mentioned earlier, a pronounced structural transition between GlbN-His and GlbN-X is inferred from the crystal structures. This reorganization involves mostly the first half of the sequence, with rigid body motions of helices B and E and rearrangement of the CE turn and the EF loop region. Inherent flexibility in these locations, as suggested at by our relaxation data, may be an essential trait for facile collective rearrangement of structural elements. The largest deviations are found for helix A and the EF loop (Figure 1C). In solution, however, the average amplitude of the changes may be smaller because conformational sampling occurs in the GlbN-His state (see colored bars in Figure 1C).

The carbonmonoxy complex achieves the same fold as GlbN-CN despite weak interactions between carbon monoxide and distal residues but appears less dynamically stable than the cyanomet complexes. What are the factors that favor the GlbN-X geometry over the GlbN-His geometry? Docking of helix A against the rest of the protein, along with favorable interactions between His46 and a heme propionate or surface side chain, is expected to stabilize the GlbN-X state. Strong interactions involving protein and an exogenous ligand appear to be necessary for rigidifying the backbone. Likewise, a strong His46−Fe bond is necessary to immobilize the backbone in the GlbN-His state. Interestingly, NMR data collected on S6803GlbN reconstituted with Zn-protoporphyrin IX (a pentacoordinate species) are not fully consistent with either the GlbN-X or GlbN-His conformation.[90] In addition, the NMR spectral properties of His46 variants of S6803GlbN[91] and GlbN[17] are indicative of heterogeneous or fluctuating structures. Steric clashes between His46 in its axial ligand orientation and the exogenous ligand therefore emerge as a driving force for the transition.

The determinants of conformational change in GlbN are interesting not only because 3/3 bis-histidine hemoglobins display a range of behavior upon exogenous ligand binding[92] but also because of the parallels that can be drawn with heme-based sensors. These proteins detect the presence of ligands such as O_2 and CO. They operate by ligand switching, reorganization of a hydrogen bond network involving the ligand, and overall changes in dynamics,[93] all of which are observed in GlbN. In fact, a sensor function is considered feasible for S6803GlbN,[94] and similarities with the globin-coupled sensor from *Geobacter sulfurreducens* have been noted.[95] However, the conformational change on ligand switching may simply be a consequence of the need to return to a bis-histidine state either to protect the heme or to facilitate electron transfer. Thus, the distinction between sensor and enzyme will require additional data, including the identification of functional partners.

■ CONCLUSIONS

A comparative analysis of six forms of GlbN has provided a unique glimpse into the dynamic behavior of a 2/2 globin. The

dx.doi.org/10.1021/bi300624a | *Biochemistry* 2012, 51, 5733−5747

heme−protein cross-link, already known to have little effect on the structure, was found to perturb backbone dynamics only modestly on the microsecond to millisecond time scales in Fe(III)GlbN-His, and not at all in Fe(III)GlbN-CN. Localized increases in Fe(II)GlbN-A-CO microsecond to millisecond motions and more widespread increases in Fe(II)GlbN-A-His pointed to a link between GlbN dynamics and the identity of the distal ligand as well as the iron oxidation state. Overall, the study emphasized the necessity of investigating multiple globin states if a relationship with function is to be sought. GlbN will present a challenging test case for protein dynamics simulations, which will need to reproduce the various effects of iron reduction and identity of the distal ligand over a time scale spanning several decades.

■ ASSOCIATED CONTENT

Supporting Information

Experimental details for NMR data collection, dipolar shift calculations, R_2 measurements at 18.8 T, and structure-based hydrodynamic modeling; 22 figures, including annotated $^1H-^{15}N$ HSQC data for each of the six GlbN forms, TALOS + results, selected NMR data documenting structural features of GlbN-X, TRACT data, Lipari−Szabo maps, R_2/R_1 ratios, HYDRONMR results, structural representations, and HX data; and four tables listing NMR delays in relaxation experiments, chemical shifts of GlnE7 and GlnE11, and R_2 selection results. This material is available free of charge via the Internet at http://pubs.acs.org.

Accession Codes

GlbN-His data associated with this work have been added as BMRB entries 16306 [Fe(III)GlbN-A-His], 16307 [Fe(III) GlbN-R-His], and 17947 [Fe(II)GlbN-A-His]. New entries containing GlbN-X data have been deposited as BMRB entries 18422 [Fe(II)GlbN-A-CO], 18423 [Fe(III)GlbN-A-CN], and 18424 [Fe(III)GlbN-R-CN].

■ AUTHOR INFORMATION

Corresponding Author

*E-mail: lecomte_jtj@jhu.edu. Phone: (410) 516-7019. Fax: (410) 516-4118.

Funding

This work was funded by National Science Foundation Grant MCB-0843439.

Notes

The authors declare no competing financial interest.

■ ACKNOWLEDGMENTS

Dr. David Vuletich contributed initial relaxation data for this work. We thank Matt Preimesberger for sharing insight into the reduced state of GlbN and comments on the text. We also thank Yagmur Muftuoglu for protein preparation and Dr. Christopher Falzone for careful reading of the manuscript. The structural representations in Figure 1 were prepared with Molscript.[96]

■ ABBREVIATIONS

azidomet GlbN, ferric GlbN with azide bound; *Ce*Hb, *C. eugametos* hemoglobin; cyanomet GlbN, ferric GlbN with cyanide bound; GlbN, *Synechococcus* sp. PCC 7002 GlbN, with or without heme post-translational modification; GlbN-A, GlbN containing a post-translationally modified *b* heme; GlbN-R, GlbN containing an intact *b* heme; met, ferric state of a globin; PDB, Protein Data Bank; PTM, post-translational modification; rmsd, root-mean-square deviation; S6803GlbN, *Synechocystis* sp. PCC 6803 GlbN.

■ REFERENCES

(1) The UniProt Consortium (2011) Reorganizing the protein space at the Universal Protein Resource (UniProt). *Nucleic Acids Res. 40*, D71−D75.

(2) Vinogradov, S. N., Hoogewijs, D., Bailly, X., Arredondo-Peter, R., Guertin, M., Gough, J., Dewilde, S., Moens, L., and Vanfleteren, J. R. (2005) Three globin lineages belonging to two structural classes in genomes from the three kingdoms of life. *Proc. Natl. Acad. Sci. U.S.A. 102*, 11385−11389.

(3) Vinogradov, S. N., and Moens, L. (2008) Diversity of globin function: Enzymatic, transport, storage, and sensing. *J. Biol. Chem. 283*, 8773−8777.

(4) Kendrew, J. C., Bodo, G., Dintzis, H. M., Parrish, R. G., Wyckoff, H., and Phillips, D. C. (1958) A three-dimensional model of the myoglobin molecule obtained by X-ray analysis. *Nature 181*, 662−666.

(5) Nardini, M., Pesce, A., Milani, M., and Bolognesi, M. (2007) Protein fold and structure in the truncated (2/2) globin family. *Gene 398*, 2−11.

(6) Hoogewijs, D., Dewilde, S., Vierstraete, A., Moens, L., and Vinogradov, S. N. (2012) A phylogenetic analysis of the globins in fungi. *PLoS ONE 7*, e31856.

(7) Ouellet, H., Ouellet, Y., Richard, C., Labarre, M., Wittenberg, B., Wittenberg, J., and Guertin, M. (2002) Truncated hemoglobin HbN protects *Mycobacterium bovis* from nitric oxide. *Proc. Natl. Acad. Sci. U.S.A. 99*, 5902−5907.

(8) Scott, N. L., Xu, Y., Shen, G., Vuletich, D. A., Falzone, C. J., Li, Z., Ludwig, M., Pond, M. P., Preimesberger, M. R., Bryant, D. A., and Lecomte, J. T. J. (2010) Functional and structural characterization of the 2/2 hemoglobin from *Synechococcus* sp. PCC 7002. *Biochemistry 49*, 7000−7011.

(9) Scott, N. L., Falzone, C. J., Vuletich, D. A., Zhao, J., Bryant, D. A., and Lecomte, J. T. J. (2002) Truncated hemoglobin from the cyanobacterium *Synechococcus* sp. PCC 7002: Evidence for hexacoordination and covalent adduct formation in the ferric recombinant protein. *Biochemistry 41*, 6902−6910.

(10) Couture, M., Das, T. K., Savard, P., Ouellet, Y., Wittenberg, J. B., Wittenberg, B. A., Rousseau, D. L., and Guertin, M. (2000) Structural investigations of the hemoglobin of the cyanobacterium *Synechocystis* PCC6803 reveal a unique distal heme pocket. *Eur. J. Biochem. 267*, 4770−4780.

(11) Scott, N. L., and Lecomte, J. T. J. (2000) Cloning, expression, purification, and preliminary characterization of a putative hemoglobin from the cyanobacterium *Synechocystis* sp. PCC 6803. *Protein Sci. 9*, 587−597.

(12) Vu, B. C., Jones, A. D., and Lecomte, J. T. J. (2002) Novel histidine−heme covalent linkage in a hemoglobin. *J. Am. Chem. Soc. 124*, 8544−8545.

(13) Falzone, C. J., Christie Vu, B., Scott, N. L., and Lecomte, J. T. J. (2002) The solution structure of the recombinant hemoglobin from the cyanobacterium *Synechocystis* sp. PCC 6803 in its hemichrome state. *J. Mol. Biol. 324*, 1015−1029.

(14) Hoy, J. A., Kundu, S., Trent, J. T., Ramaswamy, S., and Hargrove, M. S. (2004) The crystal structure of *Synechocystis* hemoglobin with a covalent heme linkage. *J. Biol. Chem. 279*, 16535−16542.

(15) Trent, J. T., III, Kundu, S., Hoy, J. A., and Hargrove, M. S. (2004) Crystallographic analysis of *Synechocystis* cyanoglobin reveals the structural changes accompanying ligand binding in a hexacoordinate hemoglobin. *J. Mol. Biol. 341*, 1097−1108.

(16) Hoy, J. A., Smagghe, B. J., Halder, P., and Hargrove, M. S. (2007) Covalent heme attachment in *Synechocystis* hemoglobin is required to prevent ferrous heme dissociation. *Protein Sci. 16*, 250−260.

(17) Nothnagel, H. J., Preimesberger, M. R., Pond, M. P., Winer, B. Y., Adney, E. M., and Lecomte, J. T. J. (2011) Chemical reactivity of *Synechococcus* sp. PCC 7002 and *Synechocystis* sp. PCC 6803 hemoglobins: Covalent heme attachment and bishistidine coordination. *J. Biol. Inorg. Chem. 16*, 539−552.
(18) Perutz, M. F., Kendrew, J., and Watson, H. (1965) Structure and function of haemoglobin. II. Some relations between polypeptide chain configuration and amino acid sequence. *J. Mol. Biol. 13*, 669−678.
(19) Vu, B. C., Nothnagel, H. J., Vuletich, D. A., Falzone, C. J., and Lecomte, J. T. J. (2004) Cyanide binding to hexacoordinate cyanobacterial hemoglobins: Hydrogen-bonding network and heme pocket rearrangement in ferric H117A *Synechocystis* hemoglobin. *Biochemistry 43*, 12622−12633.
(20) Pettersen, E. F., Goddard, T. D., Huang, C. C., Couch, G. S., Greenblatt, D. M., Meng, E. C., and Ferrin, T. E. (2004) UCSF Chimera: A visualization system for exploratory research and analysis. *J. Comput. Chem. 25*, 1605−1612.
(21) Perutz, M. F., and Mathews, F. S. (1966) An X-ray study of azide methaemoglobin. *J. Mol. Biol. 21*, 199−202.
(22) Scott, E. E., Gibson, Q. H., and Olson, J. S. (2001) Mapping the pathways for O_2 entry into and exit from myoglobin. *J. Biol. Chem. 276*, 5177−5188.
(23) Olson, J. S., Soman, J., and Phillips, G. N., Jr. (2007) Ligand pathways in myoglobin: A review of Trp cavity mutations. *IUBMB Life 59*, 552−562.
(24) Smith, R. D., Blouin, G. C., Johnson, K. A., Phillips, G. N., Jr., and Olson, J. S. (2010) Straight-chain alkyl isocyanides open the distal histidine gate in crystal structures of myoglobin. *Biochemistry 49*, 4977−4986.
(25) Vuletich, D. A., Falzone, C. J., and Lecomte, J. T. J. (2006) Structural and dynamic repercussions of heme binding and heme−protein cross-linking in *Synechococcus* sp. PCC 7002 hemoglobin. *Biochemistry 45*, 14075−14084.
(26) Pond, M. P., Vuletich, D. A., Falzone, C. J., Majumdar, A., and Lecomte, J. T. J. (2009) ^{1}H, ^{15}N, and ^{13}C resonance assignments of the 2/2 hemoglobin from the cyanobacterium *Synechococcus* sp. PCC 7002 in the ferric bis-histidine states. *Biomol. NMR Assignments 3*, 211−214.
(27) Englander, S., Calhoun, D. B., and Englander, J. J. (1987) Biochemistry without oxygen. *Anal. Biochem. 161*, 300−306.
(28) Delaglio, F., Grzesiek, S., Vuister, G., Zhu, G., Pfeifer, J., and Bax, A. (1995) NMRPipe: A multidimensional spectral processing system based on UNIX pipes. *J. Biomol. NMR 6*, 277−293.
(29) Goddard, T. D., and Kneller, D. G. (2006) *SPARKY 3*, University of California, San Francisco.
(30) Farrow, N. A., Muhandiram, R., Singer, A. U., Pascal, S. M., Kay, C. M., Gish, G., Shoelson, S. E., Pawson, T., Forman-Kay, J. D., and Kay, L. E. (1994) Backbone dynamics of a free and a phosphopeptide-complexed Src homology 2 domain studied by ^{15}N NMR relaxation. *Biochemistry 33*, 5984−6003.
(31) Piotto, M., Saudek, V., and Sklenář, V. (1992) Gradient-tailored excitation for single-quantum NMR spectroscopy of aqueous solutions. *J. Biomol. NMR 2*, 661−665.
(32) Kupče, E., and Freeman, R. (1995) Adiabatic pulses for wideband inversion and broadband decoupling. *J. Magn. Reson., Ser. A 115*, 273−276.
(33) Lee, D., Hilty, C., Wider, G., and Wüthrich, K. (2006) Effective rotational correlation times of proteins from NMR relaxation interference. *J. Magn. Reson. 178*, 72−76.
(34) Arnold, K., Bordoli, L., Kopp, J., and Schwede, T. (2006) The SWISS-MODEL workspace: A web-based environment for protein structure homology modelling. *Bioinformatics 22*, 195−201.
(35) Jesson, J. P. (1973) in *NMR of Paramagnetic Molecules; Principles and Applications* (La Mar, G. N., Horrocks, W. D., and Holm, R. H., Eds.) pp 1−52, Academic Press, New York.
(36) Emerson, S. D., and LaMar, G. N. (1990) NMR determination of the orientation of the magnetic susceptibility tensor in cyanometmyoglobin: A new probe of steric tilt of bound ligand. *Biochemistry 29*, 1556−1566.
(37) Schmitz, C., Stanton-Cook, M. J., Su, X., Otting, G., and Huber, T. (2008) Numbat: An interactive software tool for fitting $\Delta\chi$-tensors to molecular coordinates using pseudocontact shifts. *J. Biomol. NMR 41*, 179−189.
(38) Preimesberger, M. R., Pond, M. P., Majumdar, A., and Lecomte, J. T. J. (2012) Electron self-exchange and self-amplified posttranslational modification in the hemoglobins from *Synechocystis* sp. PCC 6803 and *Synechococcus* sp. PCC 7002. *J. Biol. Inorg. Chem. 17*, 599−609.
(39) Shen, Y., Delaglio, F., Cornilescu, G., and Bax, A. (2009) TALOS+: A hybrid method for predicting protein backbone torsion angles from NMR chemical shifts. *J. Biomol. NMR 44*, 213−223.
(40) Nothnagel, H. J., Winer, B. Y., Vuletich, D. A., Pond, M. P., and Lecomte, J. T. J. (2011) Structural properties of 2/2 hemoglobins: The group III protein from *Helicobacter hepaticus*. *IUBMB Life 63*, 197−205.
(41) Das, T. K., Couture, M., Ouellet, Y., Guertin, M., and Rousseau, D. L. (2001) Simultaneous observation of the O−O and Fe−O_2 stretching modes in oxyhemoglobins. *Proc. Natl. Acad. Sci. U.S.A. 98*, 479−484.
(42) Couture, M., Das, T. K., Lee, H. C., Peisach, J., Rousseau, D. L., Wittenberg, B. A., Wittenberg, J. B., and Guertin, M. (1999) *Chlamydomonas* chloroplast ferrous hemoglobin. Heme pocket structure and reactions with ligands. *J. Biol. Chem. 274*, 6898−6910.
(43) Ouellet, Y., Milani, M., Couture, M., Bolognesi, M., and Guertin, M. (2006) Ligand interactions in the distal heme pocket of *Mycobacterium tuberculosis* truncated hemoglobin N: Roles of TyrB10 and GlnE11 residues. *Biochemistry 45*, 8770−8781.
(44) Pesce, A., Couture, M., Dewilde, S., Guertin, M., Yamauchi, K., Ascenzi, P., Moens, L., and Bolognesi, M. (2000) A novel two-over-two α-helical sandwich fold is characteristic of the truncated hemoglobin family. *EMBO J. 19*, 2424−2434.
(45) La Mar, G. N., Horrocks, W. D., and Holm, R. H., Eds. (1973) *NMR of Paramagnetic Molecules; Principles and Applications*, Academic Press, New York.
(46) Berliner, L. J., and Reuben, J., Eds. (1993) *NMR Methodology for Paramagnetic Proteins*, Vol. *12*, Plenum Press, New York.
(47) Bertini, I., and Luchinat, C. (1996) in *Coordination Chemistry Reviews* (Lever, A., Ed.) Vol. *150*, Elsevier, Amsterdam.
(48) Banci, L., Bertini, I., Cavazza, C., Felli, I. C., and Koulougliotis, D. (1998) Probing the backbone dynamics of oxidized and reduced rat microsomal cytochrome b_5 via ^{15}N rotating frame NMR relaxation measurements: Biological implications. *Biochemistry 37*, 12320−12330.
(49) La Mar, G. N., and de Ropp, J. S. (1993) in *Biological Magnetic Resonance* (Berliner, L. J., and Reuben, J., Eds.) Vol. *12*, pp 1−78, Plenum Press, New York.
(50) Bertini, I., Luchinat, C., and Parigi, G. (2001) *Solution NMR of paramagnetic molecules: Applications to metallobiomolecules and models*, Elsevier, New York.
(51) Peng, J. W., and Wagner, G. (1995) Frequency spectrum of NH bonds in eglin c from spectral density mapping at multiple fields. *Biochemistry 34*, 16733−16752.
(52) Farrow, N., Zhang, O., Szabo, A., Torchia, D., and Kay, L. (1995) Spectral density function mapping using ^{15}N relaxation data exclusively. *J. Biomol. NMR 6*, 153−162.
(53) Mandel, A. M., Akke, M., and Palmer, A. G. (1995) Backbone dynamics of *Escherichia coli* ribonuclease HI: Correlations with structure and function in an active enzyme. *J. Mol. Biol. 246*, 144−163.
(54) Peng, J. W., and Wagner, G. (1969) Mapping of spectral density functions using heteronuclear NMR relaxation measurements. *J. Magn. Reson. 1992* (98), 308−332.
(55) Kroenke, C. D., Loria, J. P., Lee, L. K., Rance, M., and Palmer, A. G. (1998) Longitudinal and transverse ^{1}H−^{15}N dipolar/^{15}N chemical shift anisotropy relaxation interference: Unambiguous determination of rotational diffusion tensors and chemical exchange effects in biological macromolecules. *J. Am. Chem. Soc. 120*, 7905−7915.

(56) Tjandra, N., Wingfield, P., Stahl, S., and Bax, A. (1996) Anisotropic rotational diffusion of perdeuterated HIV protease from ^{15}N NMR relaxation measurements at two magnetic fields. *J. Biomol. NMR 8*, 273−284.
(57) García de la Torre, J., Huertas, M., and Carrasco, B. (2000) HYDRONMR: Prediction of NMR relaxation of globular proteins from atomic-level structures and hydrodynamic calculations. *J. Magn. Reson. 147*, 138−146.
(58) Lipari, G., and Szabo, A. (1982) Model-free approach to the interpretation of nuclear magnetic resonance relaxation in macromolecules. 1. Theory and range of validity. *J. Am. Chem. Soc. 104*, 4546−4559.
(59) Andrec, M., Montelione, G. T., and Levy, R. M. (2000) Lipari-Szabo mapping: A graphical approach to Lipari-Szabo analysis of NMR relaxation data using reduced spectral density mapping. *J. Biomol. NMR 18*, 83−100.
(60) Savard, P., Daigle, R., Morin, S., Sebilo, A., Meindre, F., Lagüe, P., Guertin, M., and Gagné, S. M. (2011) Structure and dynamics of *Mycobacterium tuberculosis* truncated hemoglobin N: Insights from NMR spectroscopy and molecular dynamics simulations. *Biochemistry 50*, 11121−11130.
(61) Volkman, B. F., Alam, S. L., Satterlee, J. D., and Markley, J. L. (1998) Solution structure and backbone dynamics of component IV *Glycera dibranchiata* monomeric hemoglobin−CO. *Biochemistry 37*, 10906−10919.
(62) Song, X.-J., Yuan, Y., Simplaceanu, V., Sahu, S. C., Ho, N. T., and Ho, C. (2007) A comparative NMR study of the polypeptide backbone dynamics of hemoglobin in the deoxy and carbonmonoxy forms. *Biochemistry 46*, 6795−6803.
(63) Cowley, A. B., Kennedy, M. L., Silchenko, S., Lukat-Rodgers, G. S., Rodgers, K. R., and Benson, D. R. (2006) Insight into heme protein redox potential control and functional aspects of six-coordinate ligand-sensing heme proteins from studies of synthetic heme peptides. *Inorg. Chem. 45*, 9985−10001.
(64) Barker, P. D., Ferrer, J. C., Mylrajan, M., Loehr, T. M., Feng, R., Konishi, Y., Funk, W. D., MacGillivray, R. T., and Mauk, A. G. (1993) Transmutation of a heme protein. *Proc. Natl. Acad. Sci. U.S.A. 90*, 6542−6546.
(65) Dumont, M. E., Corin, A. F., and Campbell, G. A. (1994) Noncovalent binding of heme induces a compact apocytochrome c structure. *Biochemistry 33*, 7368−7378.
(66) Barker, P. D., Nerou, E. P., Freund, S. M., and Fearnley, I. M. (1995) Conversion of cytochrome b_{562} to *c*-type cytochromes. *Biochemistry 34*, 15191−15203.
(67) Arnesano, F., Banci, L., Bertini, I., Ciofi-Baffoni, S., Woodyear, T. L., Johnson, C. M., and Barker, P. D. (2000) Structural consequences of *b*- to *c*-type heme conversion in oxidized *Escherichia coli* cytochrome b_{562}. *Biochemistry 39*, 1499−1514.
(68) Tomlinson, E. J., and Ferguson, S. J. (2000) Loss of either of the two heme-binding cysteines from a class I *c*-type cytochrome has a surprisingly small effect on physicochemical properties. *J. Biol. Chem. 275*, 32530−32534.
(69) Wain, R., Redfield, C., Ferguson, S. J., and Smith, L. J. (2004) NMR analysis shows that a *b*-type variant of *Hydrogenobacter thermophilus* cytochrome c_{552} retains its native structure. *J. Biol. Chem. 279*, 15177−15182.
(70) Assfalg, M., Banci, L., Bertini, I., Ciofi-Baffoni, S., and Barker, P. D. (2001) ^{15}N backbone dynamics of ferricytochrome b_{562}: Comparison with the reduced protein and the R98C variant. *Biochemistry 40*, 12761−12771.
(71) Dempsey, C. E. (2001) Hydrogen exchange in peptides and proteins using NMR spectroscopy. *Prog. Nucl. Magn. Reson. Spectrosc. 39*, 135−170.
(72) Geibel, J., Chang, C. K., and Traylor, T. G. (1975) Coordination of myoglobin active-site models in aqueous-solution as studied by kinetic methods. *J. Am. Chem. Soc. 97*, 5924−5926.
(73) Bondarenko, V., Dewilde, S., Moens, L., and La Mar, G. N. (2006) Solution ^{1}H NMR characterization of the axial bonding of the two His in oxidized human cytoglobin. *J. Am. Chem. Soc. 128*, 12988−12999.
(74) Giachetti, A., Penna, G. L., Perico, A., and Banci, L. (2004) Modeling the backbone dynamics of reduced and oxidized solvated rat microsomal cytochrome b_5. *Biophys. J. 87*, 498−512.
(75) Yoon, J., Herzik, M. A., Winter, M. B., Tran, R., Olea, C., and Marletta, M. A. (2010) Structure and properties of a bis-histidyl ligated globin from *Caenorhabditis elegans*. *Biochemistry 49*, 5662−5670.
(76) Collman, J. P., Brauman, J. I., Halbert, T. R., and Suslick, K. S. (1976) Nature of O_2 and CO binding to metalloporphyrins and heme proteins. *Proc. Natl. Acad. Sci. U.S.A. 73*, 3333−3337.
(77) Vangberg, T., Bocian, D. F., and Ghosh, A. (1997) Deformability of Fe(II)CO and Fe(III)CN groups in heme protein models: Nonlocal density functional theory calculations. *J. Biol. Inorg. Chem. 2*, 526−530.
(78) Sharpe, A. G., Gillard, R. D., and McCleverty, J. A. (1987) in *Comprehensive Coordination Chemistry: The Synthesis, Reactions, Properties, and Applications of Coordination Compounds* (Wilkinson, G., Ed.) 1st ed., Vol. 2, p 7, Pergamon Press, Oxford, England.
(79) Pond, M. P., Wenke, B. B., Preimesberger, M. R., Rice, S. L., and Lecomte, J. T. J. (2012) 3-Fluorotyrosine as a complementary probe of hemoglobin structure and dynamics: A ^{19}F NMR study of *Synechococcus* sp. PCC 7002 GlbN. *Chem. Biodiversity*, in press.
(80) Ludwig, M., and Bryant, D. A. (2011) Transcription profiling of the model cyanobacterium *Synechococcus* sp. strain PCC 7002 by Next-Gen (SOLiDTM) sequencing of cDNA. *Front. Microbiol. 2*, 41.
(81) Mukai, M., Ouellet, Y., Ouellet, H., Guertin, M., and Yeh, S. R. (2004) NO binding induced conformational changes in a truncated hemoglobin from *Mycobacterium tuberculosis*. *Biochemistry 43*, 2764−2770.
(82) Crespo, A., Martí, M. A., Kalko, S. G., Morreale, A., Orozco, M., Gelpi, J. L., Luque, F. J., and Estrin, D. A. (2005) Theoretical study of the truncated hemoglobin HbN: Exploring the molecular basis of the NO detoxification mechanism. *J. Am. Chem. Soc. 127*, 4433−4444.
(83) Bidon-Chanal, A., Martí, M. A., Estrin, D. A., and Luque, F. J. (2007) Dynamical regulation of ligand migration by a gate-opening molecular switch in truncated hemoglobin-N from *Mycobacterium tuberculosis*. *J. Am. Chem. Soc. 129*, 6782−6788.
(84) Lama, A., Pawaria, S., Bidon-Chanal, A., Anand, A., Gelpí, J. L., Arya, S., Martí, M., Estrin, D. A., Luque, F. J., and Dikshit, K. L. (2009) Role of pre-A motif in nitric oxide scavenging by truncated hemoglobin, HbN, of *Mycobacterium tuberculosis*. *J. Biol. Chem. 284*, 14457−14468.
(85) Daigle, R., Rousseau, J.-A., Guertin, M., and Lagüe, P. (2009) Theoretical investigations of nitric oxide channeling in *Mycobacterium tuberculosis* truncated hemoglobin N. *Biophys. J. 97*, 2967−2977.
(86) Yonetani, T., and Laberge, M. (2008) Protein dynamics explain the allosteric behaviors of hemoglobin. *Biochim. Biophys. Acta 1784*, 1146−1158.
(87) Milani, M., Pesce, A., Ouellet, Y., Ascenzi, P., Guertin, M., and Bolognesi, M. (2001) *Mycobacterium tuberculosis* hemoglobin N displays a protein tunnel suited for O_2 diffusion to the heme. *EMBO J. 20*, 3902−3909.
(88) Igarashi, J., Kobayashi, K., and Matsuoka, A. (2011) A hydrogen-bonding network formed by the B10−E7−E11 residues of a truncated hemoglobin from *Tetrahymena pyriformis* is critical for stability of bound oxygen and nitric oxide detoxification. *J. Biol. Inorg. Chem. 16*, 599−609.
(89) Daigle, R., Guertin, M., and Lagüe, P. (2009) Structural characterization of the tunnels of *Mycobacterium tuberculosis* truncated hemoglobin N from molecular dynamics simulations. *Proteins 97*, 735−747.
(90) Lecomte, J. T. J., Vu, B. C., and Falzone, C. J. (2005) Structural and dynamic properties of *Synechocystis* sp. PCC 6803 Hb revealed by reconstitution with Zn-protoporphyrin IX. *J. Inorg. Biochem. 99*, 1585−1592.
(91) Nothnagel, H. J., Love, N., and Lecomte, J. T. (2009) The role of the heme distal ligand in the posttranslational modification of *Synechocystis* hemoglobin. *J. Inorg. Biochem. 103*, 107−116.

(92) Kakar, S., Hoffman, F. G., Storz, J. F., Fabian, M., and Hargrove, M. S. (2010) Structure and reactivity of hexacoordinate hemoglobins. *Biophys. Chem. 152*, 1−14.
(93) Aono, S. (2012) Novel bacterial gas sensor proteins with transition metal-containing prosthetic groups as active sites. *Antioxid. Redox Signaling 16*, 678−686.
(94) Lukat-Rodgers, G. S., Correia, C., Botuyan, M. V., Mer, G., and Rodgers, K. R. (2010) Heme-based sensing by the mammalian circadian protein CLOCK. *Inorg. Chem. 49*, 6349−6365.
(95) Pesce, A., Thijs, L., Nardini, M., Desmet, F., Sisinni, L., Gourlay, L., Bolli, A., Coletta, M., Van Doorslaer, S., Wan, X., Alam, M., Ascenzi, P., Moens, L., Bolognesi, M., and Dewilde, S. (2009) HisE11 and HisF8 provide bis-histidyl heme hexa-coordination in the globin domain of *Geobacter sulfurreducens* globin-coupled sensor. *J. Mol. Biol. 386*, 246−60.
(96) Kraulis, P. (1991) MOLSCRIPT: A program to produce both detailed and schematic plots of protein structures. *J. Appl. Crystallogr. 24*, 946−950.